RARE METALS

Ultra-high-rate Bi anode encapsulated in 3D lignin-derived carbon framework for sodium-ion hybrid capacitors

Ze-Hua Lin, Xue-Qing Qiu* , **Xi-Hong Zu, Xiao-Shan Zhang, Lei Zhong, Shi-Rong Sun, Shu-Hua Hao, Ying-Juan Sun, Wen-Li Zhang***

Abstract Bismuth (Bi), as an alloy-based anode material, has attracted much attention in the development of sodium-ion hybrid capacitors (SIHCs) due to its high theoretical capacity. However, the volume expansion of the Bi-based anode during the sodiation/desodiation process results in limited rate capability. In the present work, a porous Bi-based composite was constructed by a one-step hydrothermal method, and Bi was encapsulated in lignin-derived nitrogen-doped porous carbon (Bi@LNPC) after carbonization. The obtained Bi nanoparticles could effectively adapt to the strain and shorten the diffusion distance of Na^+. In addition, porous carbon skeleton provides a rigid conductive network for electronic transportation. Therefore, the assembled sodium-ion half-cell with Bi@LNPC anode shows ultra-high-rate capability. When the current density was enhanced from 0.1 to 50 $A\cdot g^{-1}$, the specific capacity decreased slightly from 351.5 to 342.8 $mAh\cdot g^{-1}$. Even at an extremely high current density of 200 $A\cdot g^{-1}$, it retains 81.3% capacity retention when compared to a current density of 1 $A\cdot g^{-1}$. The SIHCs assembled by Bi@LNPC show a high energy density of 63 $Wh\cdot kg^{-1}$. This work provides an effective method for developing high-rate Bi anode materials for sodium-ion hybrid capacitors (SIHCs) and sodium-ion batteries (SIBs).

Keywords Bismuth; Lignin; Sodium-ion batteries; Sodium-ion hybrid capacitors; Rate; Porous carbon

Z.-H. Lin, X.-Q. Qiu*, X.-H. Zu, X.-S. Zhang, L. Zhong, S.-R. Sun, S.-H. Hao, W.-L. Zhang*
School of Chemical Engineering and Light Industry, Guangdong University of Technology (GDUT), Guangzhou 510006, China
e-mail: cexqqiu@scut.edu.cn

W.-L. Zhang
e-mail: wlzhang@gdut.edu.cn

X.-H. Zu, Y.-J. Sun, W.-L. Zhang
Jieyang Branch of Chemistry and Chemical Engineering Guangdong Laboratory (Rongjiang Laboratory), Jieyang 515200, China

Y.-J. Sun, W.-L. Zhang
School of Advanced Manufacturing, Institute of Green Chemistry and Advanced Materials, Guangdong University of Technology, Jieyang 515200, China

1 Introduction

Combining the benefits of capacitors and batteries, mobile-ion hybrid capacitors have become a popular topic in the electrochemical energy storage field [1]. Consequently, sodium-ion hybrid capacitors (SIHCs) have garnered significant interest due to their abundant resources, cost-effectiveness and potential high energy density. Combining a battery-type anode and a pseudocapacitive cathode, sodium-ion hybrid capacitors are desirable for their potential to deliver impressive energy density and power density [2–4]. However, the inferior performances of SIHCs are attributed to the unavailability of suitable anode materials that can accommodate the repeated insertion and extraction of large-sized sodium ions (0.097 nm) at high rates [5, 6].

Alloy-based anode materials (i.e., Sb, Sn, P and Bi) have attracted considerable attention due to their ability to deliver high sodium-ion-storage capacities [7–13]. In particular, bismuth (Bi) has a lower reaction potential (0.6 V), high theoretical specific capacity (385 $mAh\cdot g^{-1}$), and large

lattice fringes along the c-axis (0.396 nm), which is conducive to the rapid sodiation/desodiation [14, 15]. Therefore, Bi is considered to be a desirable option for commercial alloy-based anode materials of SIHCs. However, similar to other alloy-based anodes, Bi is limited by some critical issues toward practical applications. For example, the repeated insertion/extraction of sodium ions results in serious volume expansion ($\sim 244\%$), which would result in pulverization of the Bi electrode [16]. The volume expansion would therefore separate the electrode material from the current collector, and the new Bi/electrolyte interface would further consume electrolyte forming unexpected solid-electrolyte interphase (SEI), which leads to poor cycling performance. Importantly, the conductivity between Bi particles is impeded due to the breakage of Bi particles [17].

Previous investigations revealed that designing bismuth nanostructures could alleviate the significant volume expansion that occurs during the charge-discharge process [18]. Applying a conductive carbon coating could maintain the continuity between bismuth particles during the reversible sodiation/desodiation process, thus enhancing the electron transportation of Bi-based anode materials [19]. Nanostructure reduces the internal stress of bismuth particles and shortens the diffusion/transportation distance of ion/electron, resulting in a significant enhancement of the cycling stability of the Bi anode. Xu et al. designed Bi@C nanocomposites with relatively low bismuth content to improve their cycling stability [20]. Carbon-coating strategy and loading bismuth onto the carbon skeleton were used to alleviate the effect of volume expansion and the degree of pulverization, in which the carbon skeleton plays the role of providing a conductive skeleton connecting the Bi particles [21, 22]. The carbon-coated bismuth nanocomposites exhibit high stability and high-rate capability. Xue et al. fabricated the Bi@NC composite that exhibits a specific capacity of 368 mAh·g^{-1} at a current density of 2 A·g^{-1}[23]. Furthermore, the composite demonstrated a sustained specific capacity of 302 mAh·g^{-1} over 1000 cycles at a current density of 1 A·g^{-1}. Owing to the few pores in the rigid carbon skeleton, the majority of Bi/carbon composites show satisfactory rate capability; however, their cycling performance is not sustained when the current density exceeds 10 A·g^{-1}. The carbon skeleton plays a crucial role in providing a conductive network that maintains the stable connection of Bi particles during the repeated sodiation/desodiation processes of the electrode. Therefore, the construction of a carbon skeleton ensures faster sodium-ion storage dynamics and more stable cycling performance [24–26].

Lignin, the largest amount of renewable natural aromatic polymer found on the earth, serves as an ideal sustainable carbon precursor for functional carbon materials

[27]. Regrettably, lignin is predominantly burned as low-grade fuel in the paper-making industry. From the perspective of sustainable development, the conversion of lignin into electrode materials for electrochemical energy storage could facilitate the advancement of sustainable chemical engineering philosophy [28, 29]. The direct carbonization of single lignin molecule results in carbons with lower specific surface areas and inadequate 3D structures [30]. Nevertheless, by controlling the aggregation state of lignin with activation agents or guest template molecules, it is feasible to regulate the lignin to create a three-dimensional structure, thereby realizing the preparation of three-dimensional carbon materials. Our research group [31] provided a method to prepare (3D) structural carbon materials based on a supramolecule-template strategy. This approach is both straightforward and efficient, yielding a carbon material that could serve as a robust skeleton for Bi electrodes.

Herein, Bi nanocomposites encapsulated in lignin-derived nitrogen-doped porous carbon (Bi@LNPC) were synthesized as the anode material of sodium-ion batteries (SIBs) and SIHCs by a simple hydrothermal reaction and further heat treatment, with Bi nanoparticles encapsulated within a 3D carbon coating structure and incorporated into a rigid carbon framework. Through this strategy, the volume expansion of Bi nanoparticles during the charge–discharge process could be greatly reduced, enabling practical value toward commercialization. As an anode for SIHCs, Bi@LNPC electrode exhibited high-rate capability. In sodium-ion half-cell, the specific capacity remained relatively stable, with only a slight decrease from 351.5 to 342.8 mAh·g^{-1}, as the current density increased from 0.1 to 50 A·g^{-1}. Even at an extremely high current density of 200 A·g^{-1}, it still retained a capacity retention of 81.3% compared to the capacity obtained at a current density of 1 A·g^{-1}. A novel SIHCs which was composed of Bi@LNPC as the battery-type anode and activated carbon (AC) as the capacitive cathode has been successfully constructed.

2 Results and discussion

The preparation method of Bi@LNPC is illustrated in Fig. 1. Melamine (MA) and cyanuric acid (CUA) were assembled in supramolecules (MCA) through intermolecular forces in a low-temperature hydrothermal process. Meanwhile, the hydroxyl, carboxyl and sulfonic groups of sodium lignosulfonate (LS) interact with the polar groups of MCA, resulting in the uniform deposition of LS in the MCA crystal framework and mediating the aggregation of LS molecules. This approach is advantageous for constructing lignin-derived porous carbon (LNPC) with a thin carbon layer and uniform 3D pore channels. Through the
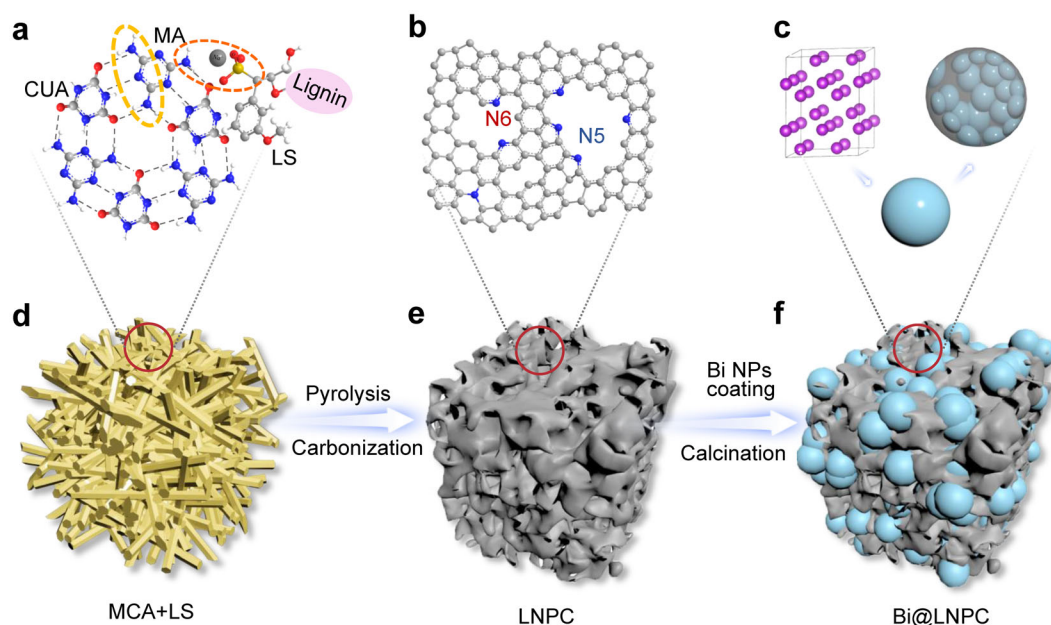
Fig. 1 Schematic illustration of synthesis of Bi@LNPC composite: molecular structure evolution of **a** MCA + LS precursor and **b** LNPC product; **c** Bi nanoparticles coated with nitrogen-doped carbon; **d–f** morphology evolution

hydrothermal method, Bi^{3+} was partially hydrolyzed to form Bi_2O_3, while also undergoing partial reduction to form metallic Bi, which was subsequently coated with a carbon layer. During the calcination process, Bi^{3+} was further reduced by carbon reduction to form metal Bi covered by a carbon layer, and Bi was loaded in the carbon skeleton forming bismuth nanospheres supported by lignin-derived porous carbon (Bi@LNPC). This innovative approach serves to mitigate the volume expansion that occurs in Bi-based electrodes during the charge–discharge processes.

2.1 Morphological analysis of LNPC and Bi@LNPC

As shown in Fig. 2a–c, LNPC displayed a 3D turbine layered structure with rich pore structure and thin carbon wall with nanometer thickness. The interaction between MCA and LS leads to the formation of a uniformly distributed entity. In the low-temperature pyrolysis process of MCA + LS precursor (Fig. S1), MCA undergoes decomposition to produce graphitic carbon nitride (g-C_3N_4), which subsequently forms covalent bonds with the amorphous carbon generated by the decomposition of LS. Under high annealing temperatures, g-C_3N_4 is decomposed due to its low structural stability. In contrast, C_3N_4 bonded with amorphous carbon exhibits higher structural stability, leading to the continuous decomposition of nitrogen-containing species. Utilizing g-C_3N_4 as a template, the decomposition of g-C_3N_4 generates pores, which enhances

the specific surface area of the carbon matrix [31]. LNPC, which has the characteristics of low density and light-weight, could significantly reduce the use of carbon support. High specific surface area could expose more active sites in the electrolyte, thereby improving the interface capacitance. The space between the porous carbon layers provides an effective buffer space for the Bi nanospheres, thereby alleviating volume expansion during the sodiation/desodiation processes. SEM images (Fig. 2d–f) show that the Bi nanosphere presents a well-formed spherical structure, and the Bi nanosphere coated with a carbon layer is evenly embedded in the 3D carbon frameworks (Fig. S2). The high-angle annular dark-field scanning TEM (HAADF-STEM) (Fig. 2g) coupled with energy dispersive spectroscopy (EDS) mapping (Fig. 2h-k) unambiguously identifies the homogeneous distribution of Bi, C, O and N in Bi@LNPC, and it also shows that the Bi nanosphere is wrapped in the nitrogen-doped carbon shell.

2.2 Physical characterization of Bi@LNPC

The crystal structures of the Bi@LNPC composite were determined by XRD measurements. All the diffraction peaks, as seen in Fig. 3a, were consistent with the standard phase of Bi (JCPDS No. 44-1246) [16, 32] and high levels of crystallinity, indicating that bismuth nitrate pentahydrate was transformed into bismuth. The graphitization degree of the carbon materials obtained was characterized through Raman spectroscopy (Fig. 3b). The presence of two prominent peaks at 69 and 98 cm^{-1}, respectively
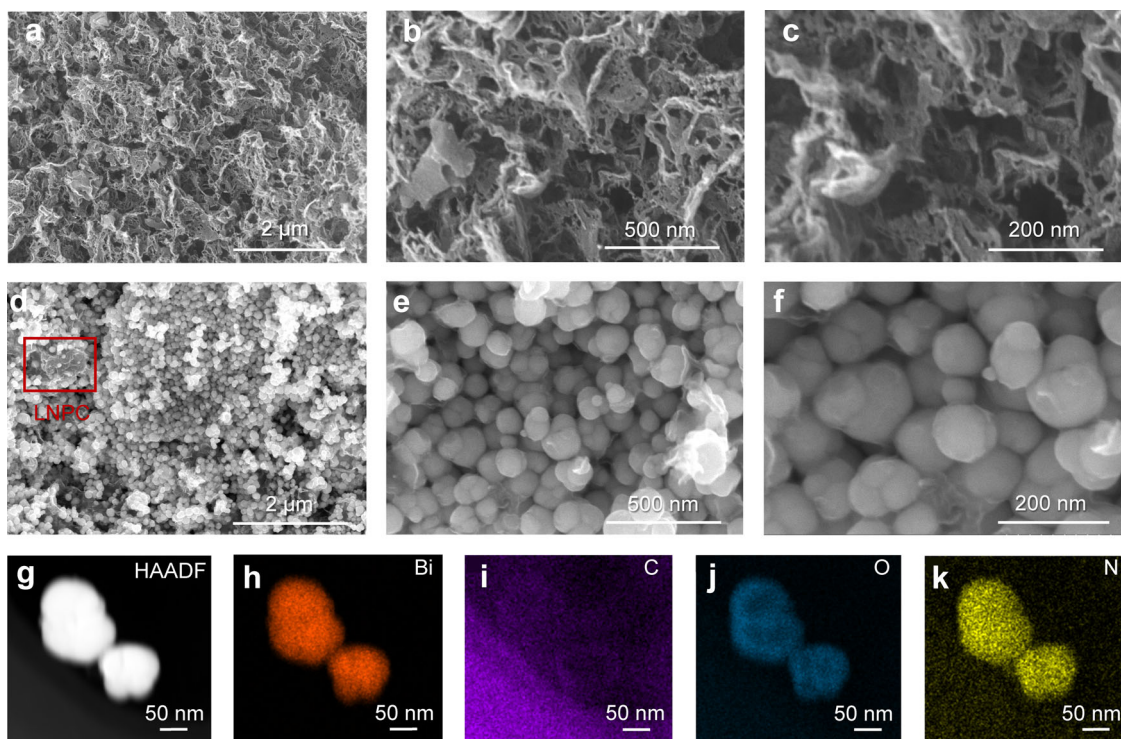
Fig. 2 Electron microscopy study of Bi@LNPC samples: SEM images of **a–c** LNPC and **d–f** Bi@LNPC; **g** HAADF image and EDS mapping of **h** Bi, **i** C, **j** O and **k** N
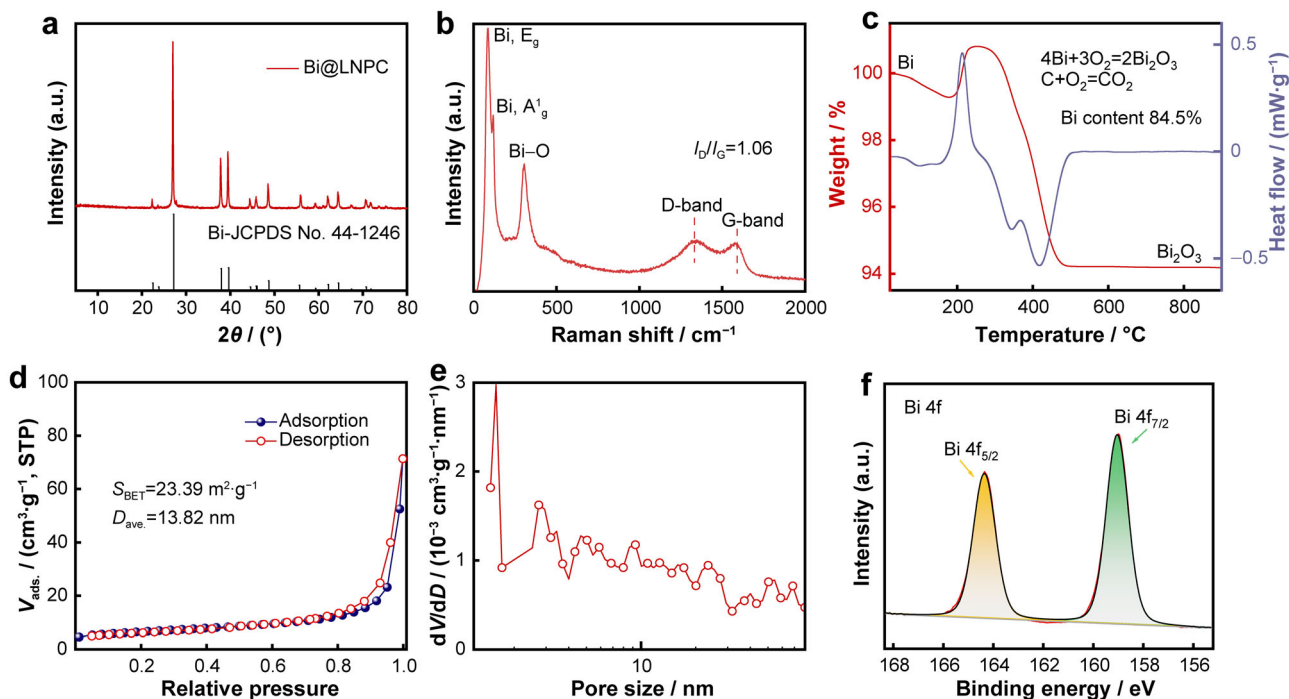

Fig. 3 Physicochemical characterizations of Bi@LNPC samples: **a** XRD patterns; **b** Raman spectra; **c** TG curves; **d** N_2 adsorption/desorption isotherm curves; **e** corresponding pore size distribution curves; **f** Bi 4f high-resolution XPS spectra

corresponding to the E_g and A^1_g peaks of rhombic bismuth structure, serves as further evidence of the successful conversion of Bi^{3+} into bismuth metal phase [33, 34]. The

high response peak observed at 311 cm^{-1} is associated with the Bi-O bond, which is attributed to the oxidation of a few Bi. The D band detected at 1329 cm^{-1} signifies the

sp^3 hybridized carbon of the carbon-based substance, whereas the G band observed at 1580 cm^{-1} indicates the sp^2 hybridized carbon [35, 36]. Moreover, the I_D/I_G ratio of 1.06 implies that the amorphous carbon shell of the Bi@LNPC contains a plethora of defects [37, 38], which could afford numerous anchoring sites for bismuth and facilitate the storage of sodium ions [39].

In order to evaluate the actual Bi content, we conducted thermogravimetric analysis (TGA) in air atmosphere (Fig. 3c). The alteration in weight can be attributed to the loss of adsorbed water, the combustion of C and N, and the oxidation of Bi. The carbonization is completed at 480 °C. By analyzing the residual product, the weight percentage of final Bi_2O_3 is 94.2%. These data lead us to conclude that the content of Bi in Bi@LNPC is ~ 84.5% (Experimental in Supporting Information). The nitrogen adsorption–desorption technique was used to check the porosity textures of the Bi@LNPC (Fig. 3d), which shows a type IV curve of H3 hysteresis ring, indicating that there is a typical physical adsorption process at mesopores and macropores. The pore size distribution curve (Fig. 3e) mainly displayed a typical mesoporous feature. The Brunauer-Emmett-Teller (BET) specific surface area of the Bi@LNPC was 23 $m^2 \cdot g^{-1}$ and the average pore size was 13.82 nm according to the adsorption volume at the relative pressure of $p/p_0 = 0.95$. Effective management of particle size at the nanometer level and carbon coating structure in electrode materials can yield significant benefits, including improved mass transfer of Na^+, enhanced conductivity of the particulate active materials, and the provision of pore space to accommodate the large volume expansion of bismuth during the charge–discharge processes. The composition and surface chemical state of Bi@LNPC were further detected by X-ray photoelectron spectroscopy (XPS). Bi@LNPC mainly includes elements of bismuth, nitrogen, carbon and oxygen (Fig. S3a). From the Bi 4f high-resolution XPS spectra (Fig. 3f), the two strong peaks located at 159.0 eV and 164.3 eV are attributed to Bi $4f_{7/2}$ and Bi $4f_{5/2}$ [23]. Compared with other literature [40–42], no other strong peaks were observed at 156.8 and 162.3 eV, indicating that there is almost no bismuth oxide formation during the material preparation process [14]. The binding energies of 284.8, 285.7 and 288.5 eV correspond to C-C, C-N and C-O bonds which can be observed in the C 1s high-resolution XPS spectra (Fig. S3b) [43]. The O 1s spectra exhibited binding energies of 529.85, 532.1 and 533.7 eV, corresponding to the Bi-O, C-O-Bi and C-O bonds, respectively, as illustrated in Fig. S3c [14]. As presented in Fig. S3d, N 1s spectrum can be divided into four characteristic peaks which are located at 398.2, 400.5, 402.8 and 403.6 eV, corresponding to pyridinic nitrogen, pyrrolic nitrogen, graphitic nitrogen, and oxidized nitrogen, respectively [44], and their relative content ratios are 39.33%, 48.57%, 4.51% and 7.59%. High edge-nitrogen can be used as active sites for Na^+, which is conducive to improving sodium-ion storage of Bi@LNPC [45].

2.3 Electrochemical performance of Bi@LNPC

Within the potential range of 0.01–1.5 V (vs. Na/Na^+), the sodium-ion storage performance of Bi@LNPC anode was investigated in a half-cell. Cyclic voltammetry (CV) reveals the existence of typical redox peaks (Fig. 4a). Seven distinct cathodic peaks at 0.17, 0.37, 0.40, 0.47, 0.59, 0.67 and 1.12 V were observed during the initial three cycles at 0.1 $mV \cdot s^{-1}$, but as the cycle progressed, the peaks of 0.17, 0.37, 0.40, 0.59 and 1.12 V gradually disappeared, which is attributed to the formation of SEI layer. The peaks of 0.47 and 0.67 V are attributed to the stepwise alloy reactions from Bi to NaBi and further to Na_3Bi, as shown below [46].

$$Bi + Na^+ + e^- \leftrightarrow NaBi \tag{1}$$

$$NaBi + 2Na^+ + 2e^- \leftrightarrow Na_3Bi \tag{2}$$

At the same time, there are two anodic peaks at 0.58 and 0.77 V which correspond to $Na_3Bi \rightarrow NaBi$ and $NaBi \rightarrow Bi$ [13]. Through the CV curves at different scan rates from 0.1 to 2.0 $mV \cdot s^{-1}$ (Fig. 4b), further discussion is made on the electrochemical kinetics of sodium-ion storage in Bi@LNPC anode. The current response of CV originates from diffusion-dominated contribution and surface-dominated contribution [47]. From the relationship between peak current and scan rate, the b value is close to 1 compared with commercial bismuth powder (cBi), indicating that the sodiation/desodiation of Bi@LNPC is a surface capacitive reaction and is not controlled by diffusion. (Fig. S4). The distribution of b value for cBi is observed to be close to 0.5, with diffusion being the dominant process influencing sodiation/desodiation (Fig. S5c) [47]. According to the results of the electrochemical impedance spectroscopy (EIS), it can be observed that Bi@LNPC exhibits a smaller circle radius in the high-frequency region than cBi (Fig. S6b). This indicates that Bi@LNPC has a lower charge transfer resistance. We attribute this lower charge transfer resistance to the continuous carbon-Bi skeleton. According to the galvanostatic intermittent titration technique (GITT) (Fig. S7), Bi@LNPC has a relatively high diffusion coefficient and a faster diffusion rate for sodium ions, which should be ascribed to the continuous framework for the efficient diffusion of sodium ions. Therefore, Bi@LNPC has better rate capabilities than cBi (Figs. S6a, S8).

The initial three galvanostatic charge–discharge (GCD) profiles of Bi@LNPC at a current density of 0.1 $A \cdot g^{-1}$ are
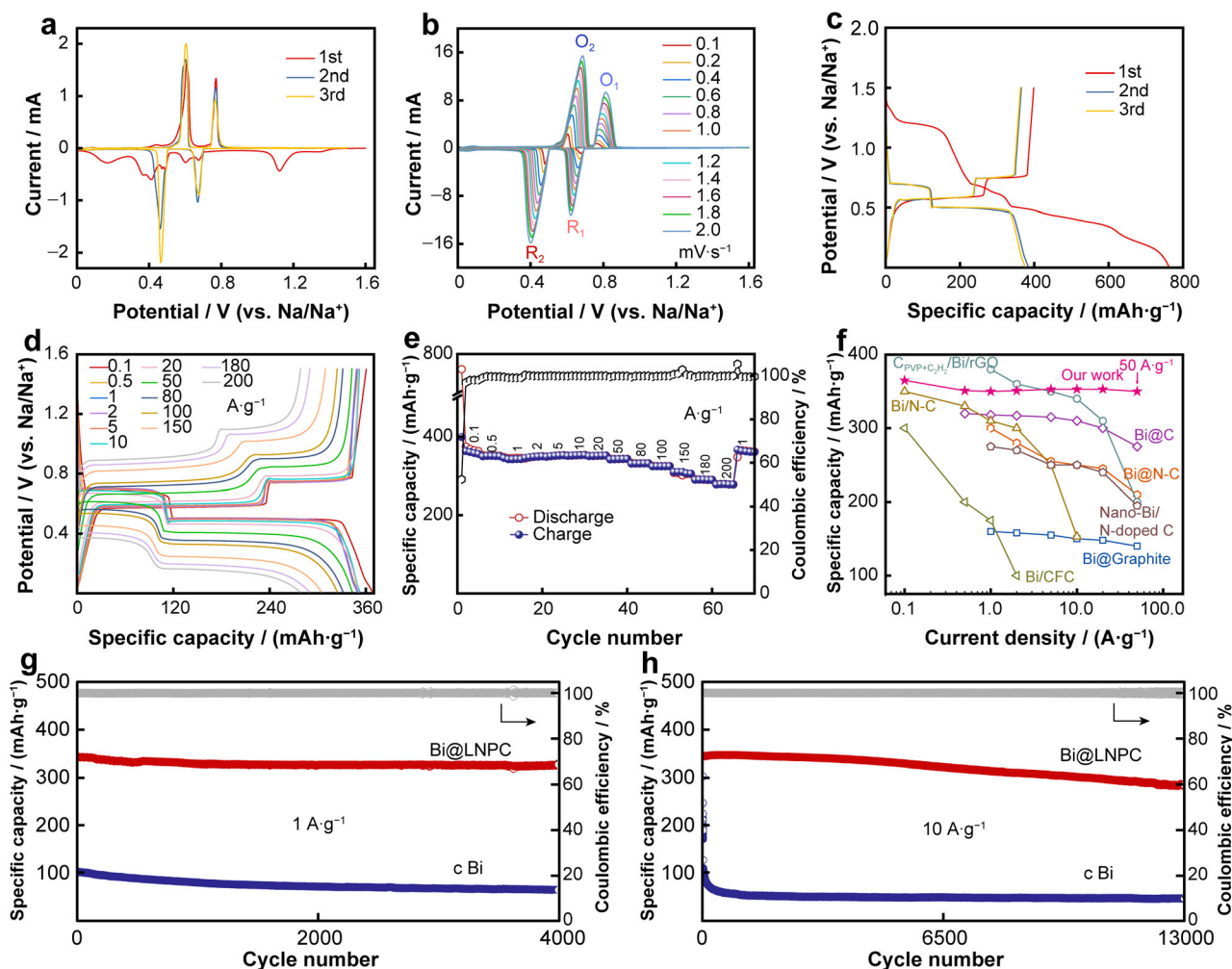
Fig. 4 Electrochemical performances of Bi@LNPC anode: **a** CV curves at a scan rate of 0.1 mV·s^{-1} between 0.01 and 1.50 V; **b** CV curves of Bi@LNPC electrode at different scan rates; **c** he GCD curves of Bi@LNPC at a current density of 0.1 A·g^{-1}; **d** GCD curves of Bi@LNPC electrode at different current densities; **e** rate performance; **f** rate capability comparison with reported Bi-based anodes materials for SIBs; cycling performance and corresponding CE at **g** 1 A·g^{-1} and **h** 10 A·g^{-1}

shown in Fig. 4c. During the initial cycle, the discharge capacity was recorded at 761.4 mAh·g^{-1} (calculated based on Bi@LNPC), while the charge capacity was 398.7 mAh·g^{-1}, resulting in an initial coulomb efficiency (ICE) of 52.4%. The main reason for the initial capacity loss was the decomposition of the electrolyte forming SEI layer and partial irreversible sodiation/desodiation process in the first cycle [48, 49]. From the second cycle, the CE demonstrates an increase toward near 100%. This suggests that the irreversible reaction only occurs in the initial stage, signifying that the material exhibits high reversibility and stable cycling performance. In the Bi@LNPC composites, Bi displays a remarkable degree of activity as evidenced by the specific charge capacity of 360.5 mAh·g^{-1} obtained after the third cycle. This value is in close to the theoretical specific capacity of Bi (385 mAh·g^{-1}). Meanwhile, there are two charge platforms situated at 0.58 and 0.77 V, in

addition to two discharge platforms located at 0.67 and 0.47 V (Fig. 4d). These platforms are associated with the reversible reaction of Na$_3$Bi $\leftrightarrow$ NaBi $\leftrightarrow$ Bi, which aligns with the CV curve. Figure 4e shows that the Bi@LNPC electrode has superior rate capability. When the current density increased from 0.1 to 20 A·g^{-1}, the specific capacity remained at 351.5 mAh·g^{-1}. Even at an extremely high current density of 50 A·g^{-1}, Bi@LNPC still provided a specific capacity of 342.8 mAh·g^{-1} (96% capacity retention with respect to 0.1 A·g^{-1}), corresponding to a charge/discharge time of $\sim$ 25 s. The specific capacity at 200 A·g^{-1} retained a capacity retention of 81.3% compared to that at a current density of 1 A·g^{-1}. Moreover, it means that it can be fully charged or discharged within a short time of 5 s. The electrochemical performance of pure LNPC was determined under the same conditions and the results showed that this carbon shows a specific capacity of

112.6 mAh·g^{-1} at 1 A·g^{-1} (Fig. S9). According to the TG-results, the carbon content of Bi@LNPC was only 15.5%. This indicates that the contribution of LNPC to the electrochemical properties of Bi@LNPC material is minimal. However, the specific capacity of cBi was less than 200 and only 70 mAh·g^{-1} at 20 A·g^{-1} (Fig. S10), which was attributed to the volume expansion of pure bismuth during charge–discharge processes forming an unstable SEI layer. Compared with the electrochemical performances of other bismuth–carbon composites in the application of SIBs (Fig. 4f), such as Bi@N-C [17], Bi@Graphite [50], Bi/CFC [51], Bi@C [52], Bi/N-C [53], C$_{pvp+C_2H_2}$/Bi/rGO [54] and nano-Bi/N-doped C [55], Bi@LNPC anode has relatively excellent electrochemical performances. Bi@LNPC showed a capacity of 325.4 mAh·g^{-1} after 4000 cycles at 1 A·g^{-1}, with a capacity retention of 95.2% (Fig. 4g). The specific capacity remained 282.6 mAh·g^{-1} after 13,000 cycles at 10 A·g^{-1} with a high capacity retention of 82.4% (Fig. 4h). The long cycle life is attributed to the robust structure of bismuth nanoparticles embedded in the nitrogen-doped carbon skeleton, which slows down the volume expansion during the charge–discharge processes. Furthermore, applying a conductive carbon coating could also maintain the continuity between bismuth particles during the reversible sodiation-desodiation process. The specific capacity of cBi electrode decreased to 62.8 mAh·g^{-1} after 4000 cycles at 1 A·g^{-1}, and the capacity retention was 61.8%. After 13,000 cycles at 10 A·g^{-1}, the specific capacity decays to 44.2 mAh·g^{-1}, with a capacity retention rate of 18.08%.

2.4 Comparison of morphology of Bi@LNPC and cBi in cycle process

The superior rate capability and cycle stability of Bi@LNPC, when compared to cBi, can be attributed to its unique morphology and robust structure evolution during the sodiation-desodiation processes (Figs. 5, S11, S12). After the initial charge-discharge cycles of Bi@LNPC, SEI layer was formed on the surface of the electrode material. For cBi, the bulk bismuth with micron sizes ultimately results in morphologies of powder and crack. With an
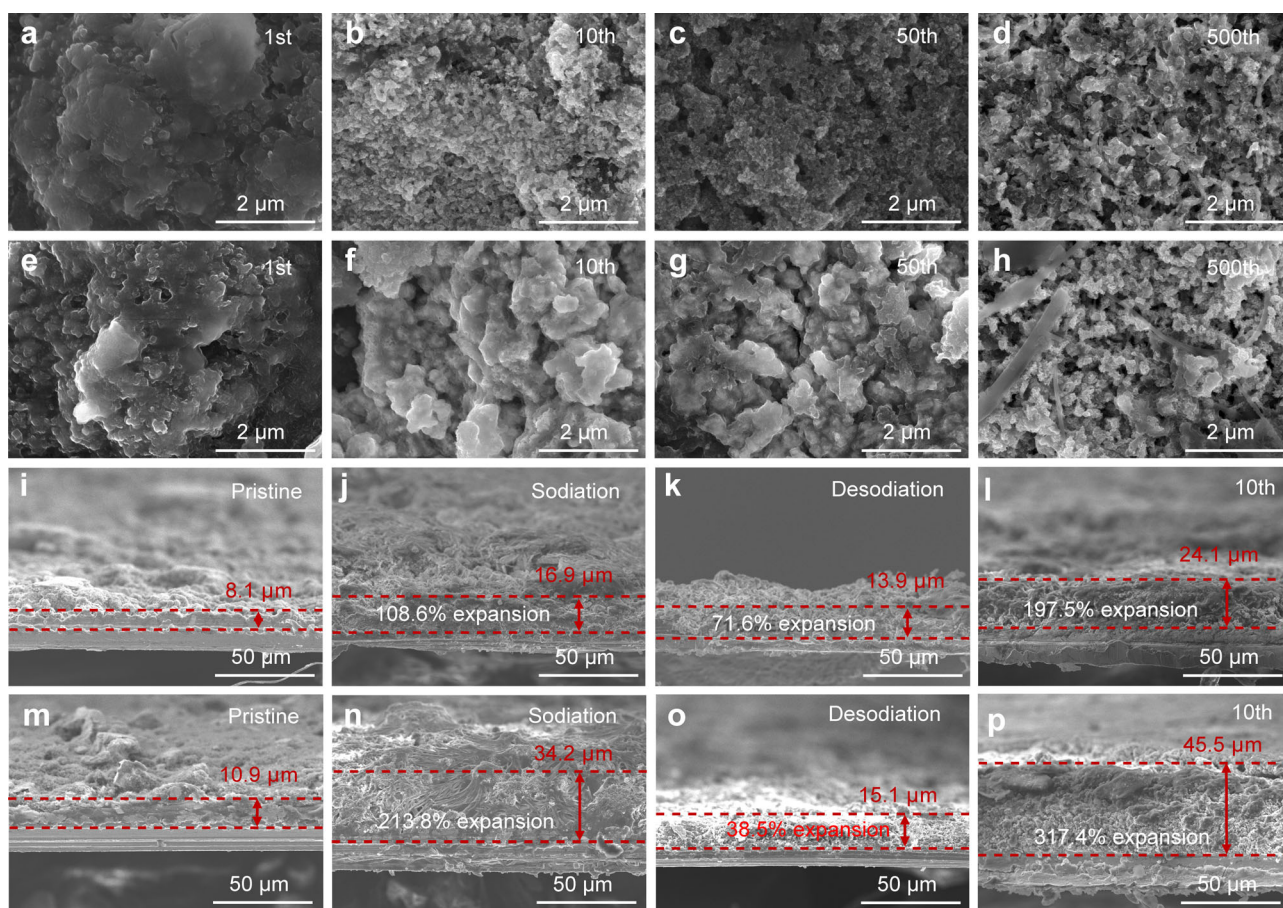

Fig. 5 SEM images of **a-d** Bi@LNPC and **e–h** cBi electrodes after 1, 10, 50 and 500 cycles; cross sectional SEM images of **i-l** Bi@LNPC anode and **m-p** cBi anode at **i, m** original, **j, n** fully sodiated, **k, o** fully desodiated states in the first cycle and **l, p** after-10-cycles states

increase in the cycle numbers, cBi was transformed into a complex 3D framework, which could be due to the wetting characteristics between Bi and electrolyte. Upon completion of 500 charge-discharge cycles, the exposed bismuth particles of cBi become were fractured (Fig. 5h), while Bi@LNPC remained in a 3D structure. During the initial cycles of the carbon-coated composites, Bi transforms into a miniature particle skeleton that facilitates rapid Na^+ insertion/extraction. To further evaluate the expansion ratios of the Bi@LNPC and the cBi anode, cross sectional SEM images of the Bi@LNPC and the cBi anode with states of pristine, sodiated, desodiated and after-10-cycles were obtained (Fig. 5i–p). The pristine electrode thickness of the two materials was almost the same, 8.1 μm and 10.9 μm, respectively. After the initial charge-discharge cycle of the Bi@LNPC in 1 mol·L^{-1} NaPF$_6$ in DME electrolyte, the sodiated and desodiated expansion ratios were 108.6% and 71.9%, respectively (Fig. 5i-l). Conversely, the corresponding values of the cBi were 213.8% and 38.5% (Fig. 5m–o). After 10 cycles, the Bi@LNPC expansion was significantly decreased when compared to that of the cBi electrode (197.5% vs. 317.4%) (Fig. 5l, p). However, no matter what the morphology Bi have, Bi still experiences volume variation, which may cause the possibility that Bi particles would disconnect. This result indicates that LNPC could buffer the volume expansion of the bismuth electrode and fall off of Bi particles during the charge-discharge processes. Compared with cBi, Bi@LNPC displayed a homogeneous and continuous framework, and its structural integrity is more stable, thus ensuring the stability of the cycling.

2.5 Sodium-ion hybrid capacitor

In order to further evaluate the potential of Bi@LNPC, its practical application was tested by assembling a SIHC (Bi@LNPC//AC). Specifically, Bi@LNPC was used as the anode electrode and YP80F (AC) as the cathode electrode, as illustrated in Fig. 6a. Before the construction of SIHC, the AC//Na sodium-ion half-cell was tested. The charge–discharge curves (Fig. S13) and CV curves (Fig. S14) of the AC cathode electrode had good symmetry, indicating that AC has a sodium-ion storage mechanism of adsorption/desorption. In addition, AC cathode electrode had the high-rate capability (Fig. S15), so AC is an excellent cathode. Considering that the side reactions generated in
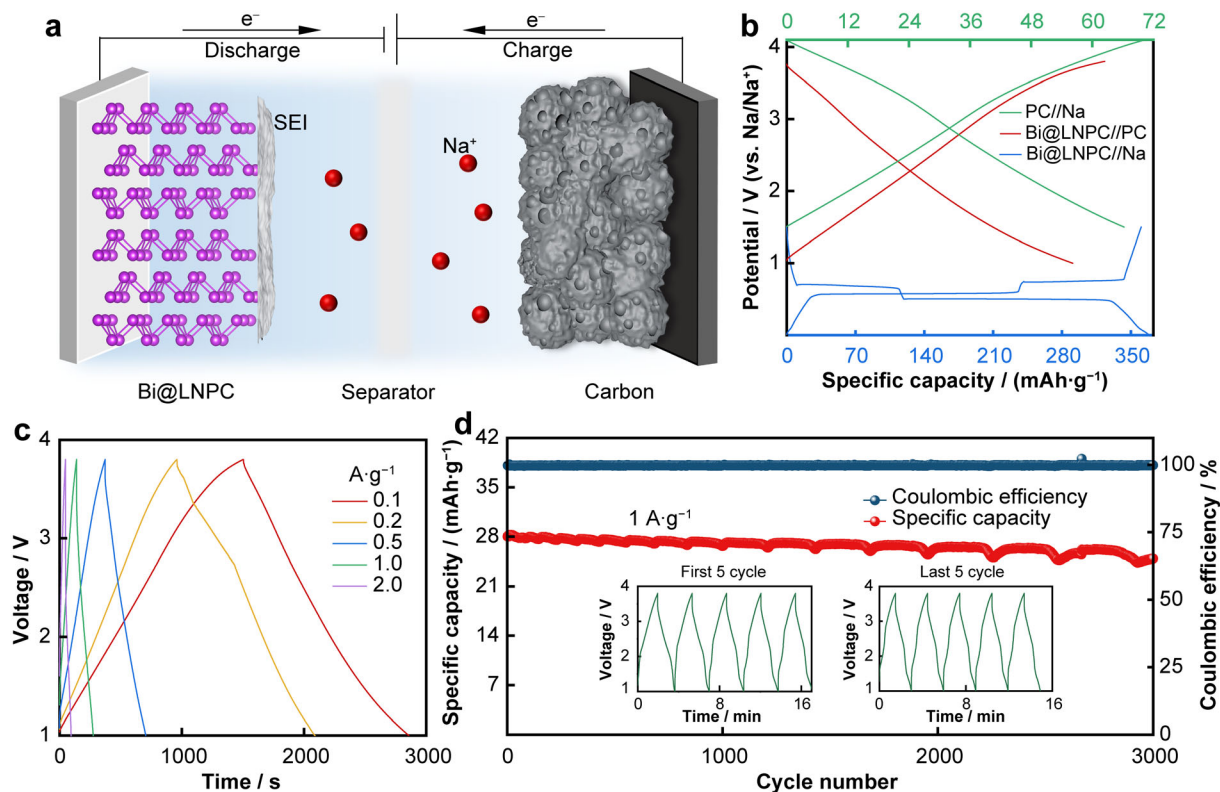

Fig. 6 Electrochemical performances of Bi@LNPC//AC SIHCs: **a** schematic illustration showing charge storage mechanism during charge and discharge processes; **b** typical GCD curves of AC cathode and Bi@LNPC anode in half cells, and Bi@LNPC//AC SIHCs; **c** GCD curves at current densities from 0.1 to 2 A·g^{-1}, dependence of gravimetric specific capacitance on GCD current densities; **d** GCD cycling performance and (insets) charge and discharge curves of the first and last five cycles

the cycling process will cause irreversible loss of sodium-ion storage, the mass ratio of Bi@LNPC with AC is 1:2.8, and the corresponding capacity ratio is 1.06:1. As shown in Fig. 6b, the electrochemical performance of Bi@LNPC//AC SIHCs was tested at a voltage window of $1-3.8$ V, and the voltage change with time of GCD is relatively symmetrical, which indicates that AC has good capacitive behavior. Figures 6c, S16 show the rate capability of SIHCs. The reversible specific capacities of Bi@LNPC//AC at 0.1, 0.2, 0.5, 1 and 2 A·g^{-1} are 73, 68, 61, 57 and 47 F·g^{-1} (calculated by the total mass of anode and cathode active substances), and the corresponding energy densities are 78, 70, 63, 46 and 25 Wh·kg^{-1}, respectively. Figure S17 shows the relationship curve between the energy density and power density of Bi@LNPC//AC. At a power density of 680 W·kg^{-1}, the corresponding energy density is 63 Wh·kg^{-1}. The energy density of Bi@LNPC//AC remains at 30 Wh·kg^{-1} after 3000 cycles at 1 A·g^{-1}, and the capacity retention is 87% (calculated based on the GCD) (Fig. 6). The excellent electrochemical performances of SIHCs are mainly attributed to the excellent electrochemical behaviors (high energy density and power density) of the anode and cathode, which fills the performance gap between the battery and the supercapacitor. The good electrochemical performances of Bi@LNPC//AC SIHCs further show that Bi@LNPC anode have potential application in SIHCs.

3 Conclusion

We prepared 3D nitrogen-doped carbon skeleton from lignin using a supramolecule-template strategy. This carbon allowed us to synthesize a porous bismuth-carbon composite through combined hydrothermal and carbonization processes. Upon carbonization, Bi is encapsulated within the lignin-derived porous carbon, resulting in the formation of Bi@LNPC. This innovative approach effectively mitigates the volume variation of bismuth particles, shortens the diffusion distance of ion/electron, which enhances the rate capability of the material. At the same time, LNPC can be used as a rigid framework to improve the conductivity of the nanoparticles in Bi composite electrodes. Therefore, the Bi@LNPC anode in SIBs and SIHCs shows ultra-high-rate capability. This work provides guidance for the application of high-rate Bi-based anode in high-rate SIBs and SIHCs.

Declarations

Conflict of interests The authors declare that they have no conflict of interest.

References

[1] Jian WB, Zhang WL, Wu BC, Wei XE, Liang WL, Zhang XS, Wen FW, Zhao L, Yin J, Lu K, Qiu XQ. Enzymatic hydrolysis lignin-derived porous carbons through ammonia activation: activation mechanism and charge storage mechanism. ACS Appl Mater Interfaces. 2022;14(4):5425. https://doi.org/10.1021/acsami.1c22576.

[2] Sun YY, Li SQ, Wang CR, Qian YX, Zheng SY, Yuan T. Research progress layered transition metal oxide cathode materials for sodium ion batteries. Chin J Rare Met. 2022;46(6):776. https://doi.org/10.13373/j.cnki.cjrm.XY22020014.

[3] Xiao Y, Wang HR, Hu HY, Zhu YF, Li S, Li JY, Wu XW, Chou SL. Formulating high-rate and long-cycle heterostructured layered oxide cathodes by local chemistry and orbital hybridization modulation for sodium-ion batteries. Adv Mater. 2022;34(33):2202695. https://doi.org/10.1002/adma.202202695.

[4] Dong SY, Wu YL, Lv N, Ren RQ, Huang L. Porous sodium titanate nanofibers for high energy quasi-solid-state sodium-ion hybrid capacitors. Rare Met. 2022;41(7):2453. https://doi.org/10.1007/s12598-022-02002-4.

[5] Sun JH, Sadd M, Edenborg P, Grönbeck H, Thiesen PH, Xia ZY, Quintano V, Qiu R, Matic A, Palermo V. Real-time imaging of Na$^+$ reversible intercalation in "Janus" graphene stacks for battery applications. Sci Adv. 2021;7(22):eabf0812. https://doi.org/10.1126/sciadv.abf0812.

[6] Ramachandran K, Subburam G, Liu XH, Huang MG, Xu C, Ng DHL, Cui YX, Li GC, Qiu JX, Wang C, Lian JB. Nitrogen-doped porous carbon nanofoams with enhanced electrochemical kinetics for superior sodium-ion capacitor. Rare Met. 2022;41(7):2481. https://doi.org/10.1007/s12598-022-01992-5.

[7] Lei KX, Wang CC, Liu LJ, Luo YW, Mu CN, Li FJ, Chen J. A porous network of bismuth used as the anode material for high-energy-density potassium-ion batteries. Angew Chem Int Ed. 2018;57(17):4687. https://doi.org/10.1002/anie.201801389.

[8] Sun XZ, Wang CL, Gong Y, Gu L, Chen QW, Yu Y. A flexible sulfur-enriched nitrogen doped multichannel hollow carbon nanofibers film for high performance sodium storage. Small. 2018;14(35):1802218. https://doi.org/10.1002/smll.201802218.

[9] Li WH, Hu SH, Luo XY, Li ZL, Sun XZ, Li MS, Liu FF, Yu Y. Confined amorphous red phosphorus in MOF-derived N-doped microporous carbon as a superior anode for sodium-ion battery. Adv Mater. 2017;29(16):1605820. https://doi.org/10.1002/adma.201605820.

[10] Wu TJ, Zhang CY, Hou HS, Ge P, Zou GQ, Xu W, Li SM, Huang ZD, Guo TX, Jing MJ, Ji XB. Dual functions of potassium antimony(III)-tartrate in tuning antimony/carbon composites for long-life Na-ion batteries. Adv Funct Mater. 2018;28(10):1705744. https://doi.org/10.1002/adfm.201705744.

[11] Xiong PX, Bai PX, Tu SB, Cheng MR, Zhang JF, Sun J, Xu YH. Red phosphorus nanoparticle@3D interconnected carbon nanosheet framework composite for potassium-ion battery anodes. Small. 2018;14(33):1802140. https://doi.org/10.1002/smll.201802140.

[12] Zhou XS, Yu L, Yu XY, Lou XW. Encapsulating Sn nanoparticles in amorphous carbon nanotubes for enhanced lithium

storage properties. Adv Energy Mater. 2016;6(22):1601177. https://doi.org/10.1002/aenm.201601177.

[13] Wang CC, Wang L, Li F, Cheng F, Chen J. Bulk bismuth as a high-capacity and ultralong cycle-life anode for sodium-ion batteries by coupling with glyme-based electrolytes. Adv Mater. 2017;29(35):1702212. https://doi.org/10.1002/adma.201702212.

[14] Zhang Q, Mao JF, Pang WK, Zheng T, Sencadas V, Chen YZ, Liu YJ, Guo ZP. Boosting the potassium storage performance of alloy-based anode materials via electrolyte salt chemistry. Adv Energy Mater. 2018;8(15):1703288. https://doi.org/10.1002/aenm.201703288.

[15] Yin H, Li QW, Cao ML, Zhang W, Zhao H, Li C, Huo K, Zhu MQ. Nanosized-bismuth-embedded 1D carbon nanofibers as high-performance anodes for lithium-ion and sodium-ion batteries. Nano Res. 2017;10(6):2156. https://doi.org/10.1007/s12274-016-1408-z.

[16] Zhou J, Chen JC, Chen MX, Wang J, Liu XZ, Wei B, Wang ZC, Li JJ, Gu L, Zhang QH, Wang H, Guo L. Few-layer bismuthene with anisotropic expansion for high-areal-capacity sodium-ion batteries. Adv Mater. 2019;31(12):1807874. https://doi.org/10.1002/adma.201807874.

[17] Yang H, Xu R, Yao Y, Ye SF, Zhou XF, Yu Y. Multicore–shell Bi@N-doped carbon nanospheres for high power density and long cycle life sodium- and potassium-ion anodes. Adv Funct Mater. 2019;29(13):1809195. https://doi.org/10.1002/adfm.201809195.

[18] Yang FH, Yu F, Zhang ZA, Zhang K, Lai YQ, Li J. Bismuth nanoparticles embedded in carbon spheres as anode materials for sodium/lithium-ion batteries. Chem Eur J. 2016;22(7):2333. https://doi.org/10.1002/chem.201503272.

[19] Chen L, He XJ, Chen HM, Huang SP, Wei MD. N-doped carbon encapsulating Bi nanoparticles derived from metal-organic frameworks for high-performance sodium-ion batteries. J Mater Chem A. 2021;9(38):22048. https://doi.org/10.1039/D1TA06558K.

[20] Xiong PX, Bai PX, Li A, Li BF, Cheng MR, Chen YP, Huang SP, Jiang Q, Bu X-H, Xu YH. Bismuth nanoparticle@carbon composite anodes for ultralong cycle life and high-rate sodium-ion batteries. Adv Mater. 2019;31(48):1904771. https://doi.org/10.1002/adma.201904771.

[21] Cai R, Zhang WQ, Zhou JH, Yang KS, Sun LF, Yang L, Ran LG, Shao RW, Fukuda T, Tan GQ, Liu HD, Wan JY, Zhang QB, Dong LX. Unraveling atomic-scale origins of selective Ionic transport pathways and sodium-ion storage mechanism in Bi_2S_3 anodes. Small Methods. 2022;6(11):2200995. https://doi.org/10.1002/smtd.202200995.

[22] Zhang XS, Qiu XQ, Lin JX, Lin ZH, Sun SR, Yin J, Alshareef HN, Zhang WL. Structure and interface engineering of ultra-high-rate 3D bismuth anodes for sodium-ion batteries. Small. 2023. https://doi.org/10.1002/smll.202302071.

[23] Xue P, Wang NN, Fang ZW, Lu ZX, Xu X, Wang L, Du Y, Ren XC, Bai ZC, Dou SX, Yu GH. Rayleigh-instability-induced bismuth nanorod@nitrogen-doped carbon nanotubes as a Long cycling and high rate anode for sodium-ion batteries. Nano Lett. 2019;19(3):1998. https://doi.org/10.1021/acs.nanolett.8b05189.

[24] Fang YJ, Yu XY, Lou XW. Bullet-like Cu_9S_5 Hollow particles coated with nitrogen-doped carbon for sodium-ion batteries. Angew Chem Int Ed. 2019;58(23):7744. https://doi.org/10.1002/anie.201902988.

[25] Fang YJ, Luan DY, Chen Y, Gao SY, Lou XW. Rationally designed three-jayered Cu_2S@Carbon@MoS_2 hierarchical nanoboxes for efficient sodium storage. Angew Chem Int Ed. 2020;59(18):7178. https://doi.org/10.1002/anie.201915917.

[26] Liang K, Ren YR. Stabilization of Sb nanoparticles using metal-organic frameworks to obtain stable performance of anode

[27] material for sodium-ion batteries. Rare Met. 2022;41(5):1406. https://doi.org/10.1007/s12598-021-01924-9.

Wang SC, Bai JX, Innocent MT, Wang QQ, Xiang HX, Tang JG, Zhu MF. Lignin-based carbon fibers: formation, modification and potential applications. Green Energy Environ. 2022;7(4):578. https://doi.org/10.1016/j.gee.2021.04.006.

[28] Ragauskas AJ, Beckham GT, Biddy MJ, Chandra R, Chen F, Davis MF, Davison BH, Dixon RA, Gilna P, Keller M, Langan P, Naskar AK, Saddler JN, Tschaplinski TJ, Tuskan GA, Wyman CE. Lignin valorization: improving lignin processing in the biorefinery. Science. 2014;344(6185):1246843. https://doi.org/10.1126/science.1246843.

[29] Liu HY, Xu T, Liu K, Zhang M, Liu W, Li H, Du HS, Si CL. Lignin-based electrodes for energy storage application. Ind Crops Prod. 2021;165: 113425. https://doi.org/10.1016/j.indcrop.2021.113425.

[30] Sun ZZ, Dai LC, Lai PH, Shen F, Shen F, Zhu WK. Air oxidation in surface engineering of biochar-based materials: a critical review. Carbon Res. 2022;1(1):32. https://doi.org/10.1007/s44246-022-00031-3.

[31] Zhang WL, Yin J, Jian WB, Wu Y, Chen LH, Sun ML, Schwingenschlögl U, Qiu XQ, Alshareef HN. Supermolecule-mediated defect engineering of porous carbons for zinc-ion hybrid capacitors. Nano Energy. 2022;103: 107827. https://doi.org/10.1016/j.nanoen.2022.107827.

[32] Wei CH, Guo SG, Ma W, Mei SX, Xiang B, Gao B. Recent progress of bismuth-based electrode materials for advanced sodium ion batteries anode. Chin J Rare Met. 2021;45(5):611. https://doi.org/10.13373/j.cnki.cjrm.XY20070021.

[33] Wang WZ, Liu MJ, Yang ZX, Mai WJ, Gong JT. Synthesis and raman optical properties of single-crystalline Bi nanowires. Physica E Low Dimens Syst Nanostruct. 2012;44(7–8):1142. https://doi.org/10.1016/j.physe.2012.01.001.

[34] Bai XY, Li SS, Das S, Du LJ, Dai YY, Yao LD, Raju R, Du MD, Lipsanen H, Sun ZP. Single-step chemical vapour deposition of anti-pyramid MoS_2/WS_2 vertical heterostructures. Nanoscale. 2021;13(8):4537. https://doi.org/10.1039/d0nr08281c.

[35] Ma H, Wang T, Li J, Yang J, Liu Z, Wang N, Su D, Wang C. Nitrogen doped carbon coated bi microspheres as high-performance anode for half and full sodium ion batteries. Chem Asian J. 2021. https://doi.org/10.1002/asia.202100519.

[36] Zhong YT, Li B, Li SM, Xu SY, Pan ZH, Huang QM, Xing LD, Wang CS, Li WS. Bi nanoparticles anchored in N-doped porous carbon as anode of high energy density lithium ion battery. Nanomicro Lett. 2018;10:56. https://doi.org/10.1007/s40820-018-0209-1.

[37] Cheng XL, Li DJ, Wu Y, Xu R, Yu Y. Bismuth nanospheres embedded in three-dimensional (3D) porous graphene frameworks as high performance anodes for sodium- and potassium-ion batteries. J Mater Chem A. 2019;7(9):4913. https://doi.org/10.1039/C8TA11947C.

[38] Hong WW, Ge P, Jiang YL, Yang L, Tian Y, Zou GQ, Cao XY, Hou HS, Ji XB. Yolk-shell-structured bismuth@N-doped carbon anode for lithium-ion battery with high volumetric capacity. ACS Appl Mater Interfaces. 2019;11(11):10829. https://doi.org/10.1021/acsami.8b20477.

[39] Wu DX, Wang CY, Wu MG, Chao YF, He PB, Ma JM. Porous bowl-shaped VS_2 nanosheets/graphene composite for high-rate lithium-ion storage. J Energy Chem. 2020;43:24. https://doi.org/10.1016/j.jechem.2019.08.003.

[40] Zhang F, Liu XJ, Wang BB, Wang G, Wang H. Bi@C nanospheres with the unique petaloid core-shell structure anchored on porous graphene nanosheets as an anode for stable sodium- and potassium-ion batteries. ACS Appl Mater Interfaces. 2021;13(50):59867. https://doi.org/10.1021/acsami.1c16946.

[41] Cui RC, Zhou HY, Li JC, Yang CC, Jiang Q. Ball-cactus-like Bi embedded in N-riched carbon nanonetworks enables the best potassium storage performance. Adv Funct Mater. 2021;31(33): 2103067. https://doi.org/10.1002/adfm.202103067.

[42] Chen KT, Tuan HY. Bi-Sb nanocrystals embedded in phosphorus as high-performance potassium ion battery electrodes. ACS Nano. 2020;14(9):11648. https://doi.org/10.1021/acsnano.0c04203.

[43] Guo QB, Ma YF, Chen TT, Xia QY, Yang M, Xia H, Yu Y. Cobalt sulfide quantum dot embedded N/S-doped carbon nanosheets with superior reversibility and rate capability for sodium-ion batteries. ACS Nano. 2017;11(12):12658. https://doi.org/10.1021/acsnano.7b07132.

[44] Shi XL, Zhang JS, Yao QQ, Wang R, Wu HF, Zhao Y, Guan LH. A self-template approach to synthesize multicore–shell Bi@N-doped carbon nanosheets with interior void space for high-rate and ultrastable potassium storage. J Mater Chem A. 2020;8(16):8002. https://doi.org/10.1039/C9TA13975C.

[45] Wang XX, Wu Y, Huang P, Chen P, Wang ZY, Xu XW, Xie J, Yan J, Li SG, Tu J, Ding YL. A multi-layered composite assembly of Bi nanospheres anchored on nitrogen-doped carbon nanosheets for ultrastable sodium storage. Nanoscale. 2020; 12(46):23682. https://doi.org/10.1039/D0NR07230C.

[46] Liang YZ, Song N, Zhang ZCY, Chen WH, Feng JK, Xi BJ, Xiong SL. Integrating Bi@C nanospheres in porous hard carbon frameworks for ultrafast sodium storage. Adv Mater. 2022; 34(28):2202673. https://doi.org/10.1002/adma.202202673.

[47] Zhong L, Zhang WL, Sun SR, Zhao L, Jian WB, He X, Xing ZY, Shi ZX, Chen YN, Alshareef HN, Qiu XQ. Engineering of the crystalline lattice of hard carbon anodes toward practical potassium-ion batteries. Adv Funct Mater. 2022;33(8):2211872. https://doi.org/10.1002/adfm.202211872.

[48] Yang H, Chen LW, He FX, Zhang JQ, Feng YZ, Zhao LK, Wang B, He LX, Zhang QB, Yu Y. Optimizing the void size of yolk-shell Bi@Void@C nanospheres for high-power-density sodium-ion batteries. Nano Lett. 2020;20(1):758. https://doi.org/10.1021/acs.nanolett.9b04829.

[49] Wang YX, Wang YX, Wang Y-X, Feng XM, Chen WH, Qian JF, Ai XP, Yang HX, Cao YL. In situ formation of Co$_9$S$_8$ nanoclusters in sulfur-doped carbon foam as a sustainable and high-rate sodium-ion anode. ACS Appl Mater Interfaces. 2019; 11(21):19218. https://doi.org/10.1021/acsami.9b05134.

[50] Chen J, Fan XL, Ji X, Gao T, Hou S, Zhou XQ, Wang LN, Wang F, Yang CY, Chen L, Wang CS. Intercalation of Bi nanoparticles into graphite results in an ultra-fast and ultra-stable anode material for sodium-ion batteries. Energy Environ Sci. 2018; 11(5):1218. https://doi.org/10.1039/c7ee03016a.

[51] Liu SN, Luo ZG, Guo JH, Pan AQ, Cai ZY, Liang SQ. Bismuth nanosheets grown on carbon fiber cloth as advanced binder-free anode for sodium-ion batteries. Electrochem commun. 2017;81: 10. https://doi.org/10.1016/j.elecom.2017.05.011.

[52] Li ZH, Zhong WH, Cheng DJ, Zhang HY. One-step large-scale fabrication of Bi@N-doped carbon for ultrahigh-rate and long-life sodium-ion battery anodes. J Mater Sci. 2021;56: 11000. https://doi.org/10.1007/s10853-021-05978-z.

[53] Wang LB, Voskanyan AA, Chan KY, Qin B, Li FJ. Combustion synthesized porous bismuth/N-doped carbon nanocomposite for reversible sodiation in a sodium-ion battery. ACS Appl Mater Interfaces. 2020;3(1):565. https://doi.org/10.1021/acsaem.9b01799.

[54] Hu CJ, Zhu YS, Ma GY, Tian F, Zhou YL, Yang J, Qian YT. Sandwich-structured dual carbon modified bismuth nanosphere composites as long-cycle and high-rate anode materials for sodium-ion batteries. Electrochim Acta. 2021;365: 137379. https://doi.org/10.1016/j.electacta.2020.137379.

[55] Zhong X, Chen YW, Zhang W, Zhang ZW, Li MQ. Facile synthesis of a honeycomb-like nano-Bi/N-Doped C composite as an anode for sodium-ion batteries with superb cycle stability. ACS Sustain Chem Eng. 2022;10(27):8856. https://doi.org/10.1021/acssuschemeng.2c01798.